*International Journal of Remote Sensing*
*Geerling, G.W.* et al.
*Data-fusion of Spectral (CASI) and LiDAR data*

**Research Article**

# Classification of floodplain vegetation by data-fusion of Spectral (CASI) and LiDAR data

G.W. GEERLING∗†#, M. LABRADOR-GARCIA‡, J.G.P.W. CLEVERS‡, A.M.J. RAGAS§# AND A.J.M. SMITS †#

† CSMR, Institute for Science, Innovation and Society (ISIS), Faculty of Science, Radboud University. P.O. Box 9010, 6500 GL Nijmegen. The Netherlands.

‡ Centre for Geo-Information, Wageningen University and Research Centre, P.O. Box 47, 6700 AA Wageningen, The Netherlands.

§ Department of Environmental Science, Institute for Water and Wetland Research (IWWR), Faculty of Science, Radboud University. P.O. Box 9010, 6500 GL Nijmegen. The Netherlands.

# Member of the Netherlands Centre for River Studies (NCR), P.O. Box 177, 2600 MH Delft, The Netherlands.

Abstract

To safeguard the goals of flood protection and nature development, a river manager requires detailed and up-to-date information on vegetation structures in floodplains. In this study, remote sensing data on the vegetation of a semi-natural floodplain along the river Waal in the Netherlands was gathered by means of a Compact Airborne Spectrographic Imager (CASI; spectral information) and LiDAR (structural information). This data was used to classify the floodplain vegetation into 8 and 5 different vegetation classes, respectively. The main objective was to fuse the CASI and LiDAR-derived datasets on a pixel level, and to compare the classification results of the fused dataset with those of the non-fused datasets. The performance of the classification results was evaluated against vegetation data recorded in the field. The LiDAR data alone provided insufficient information for accurate classification. The overall accuracy amounted to 41% in the 5-class set. Using CASI data only, the overall accuracy was 74% (5-class set). The combination produced the best results, raising the overall accuracy to 81% (5-class set). It is concluded that fusion of CASI and LiDAR data can improve the classification of floodplain vegetation, especially for those vegetation classes which are important to predict hydraulic roughness, i.e. bush and forest. A novel measure, the balance index, is introduced to assess the accuracy of error matrices describing an ordered sequence of classes such as vegetation structure classes that range from bare soil to forest.

---

∗∗ Corresponding author. Email: Gertjan.Geerling@science.ru.nl

*Keywords:* Vegetation mapping; Rhine; CASI; LiDAR; Data fusion; Maximum Likelihood Classification.

## 1. Introduction

Climate change is expected to result into more extreme peak discharges in large Western European rivers, particularly in winter. The floods of the river Rhine in 1993 and 1995 and of the river Oder in 1997 show the limited capacity of these main rivers to accommodate present peak discharges. To increase the discharge capacity, embanked floodplains in use by farmers have been restructured to accommodate higher peak discharges and are at the same time designated as nature rehabilitation site (Smits *et al.* 2000, Wolfert 2001, Lenders, 2003, van der Velde *et al.* 2006). Due to this management change, the floodplain vegetation will change over time (Bekhuis *et al.* 1995, Prach and Pysek 2001, Sýkora 2002, Geerling *et al.* 2006).

Accurate and up-to-date information on this dynamic vegetation is of vital importance to the river manager because the maximum discharge capacity depends on it through its hydraulic resistance. If the discharge capacity becomes too low, special measures are necessary, e.g. removal of bushes and softwood forests. A readily available, labour efficient, reliable and cost effective instrument to monitor the floodplain vegetation for hydraulic and ecological evaluation is needed (Geerling and Van den Berg 2002, Dowling and Accad 2003, Turner *et al.* 2003, Baptist *et al.* 2004). This paper explores the possibilities of digital remote sensing techniques to monitor and classify semi-natural floodplain vegetation (Leuven *et al.* 2002).

Two promising techniques to remotely sense vegetation are imaging spectroscopy (IS) and the Light Detection And Ranging (LiDAR) sensor technology. With IS spectral information (reflected sunlight) in the visible and shortwave Infra Red (IR) range is collected. In the current study we used the Compact Airborne Spectrographic Imager (CASI). This sensor has been used in several studies for high resolution vegetation mapping (Kurnatowska 1998, Shang *et al.* 1998, Protz *et al.* 1999, Von Hansen and Sties 2000, Leckie *et al.* 2005). On the basis of spectral information alone especially bush and forest types were confused (Geerling and Van den Berg 2002). The distinction between these vegetation classes is important because they differ considerably in hydraulic resistance.

LiDAR was originally introduced to facilitate the collection of data for digital elevation models (DEMs, Ackermann 1999, Wehr and Lohr 1999, Lillesand and Kiefer 2000, Charlton *et al.* 2003). In the process of creating a DEM, only reflections from the ground level are used and reflections from vegetation are considered redundant. Recent studies with LiDAR data have explored the possibilities to use these redundant vegetation reflections to map vertical vegetation structures. The results can be applied in woodland management (tree density, timber volume, tree height) and ecological (habitat) mapping (Protz *et al.* 1999, Zimble *et al.* 2003, Hill and Thompson 2005, Suárez *et al.* 2005, Straatsma and Middelkoop 2006). Studies to map riparian vegetation using LiDAR showed that discrimination of some vegetation types was possible based on vegetation height and density. The vegetation types that were similar in structure (e.g. bare soil and short grassland) were difficult to separate, but discrimination between bushes and trees was high (Asselman 2001, Cobby *et al.* 2001, Asselman *et al.* 2002, Dowling and Accad 2003). In this paper LiDAR will be used both for the technique and for the instrument used.

Based on the above, the IS and LiDAR data seem complementary. As suggested by Leckie *et al.* (2005), the use of both data types in one classification could be synergetic. This idea is called data fusion. Pohl and van Genderen (1998) describe three types of data fusion: data-fusion at the

decision level, at the feature level and at the pixel level. When datasets are fused at the decision level, they are processed completely separately and only the end results (say maps) are "fused" by combination in a GIS. Ordinary GIS overlays already qualify for this level of data fusion. At the feature level, the datasets are processed individually, resulting in unidentified features. The identification of the features is done by combining feature information of the two datasets. Finally, at the pixel level, the datasets are fused immediately and processed together to produce the end result.

Hill *et al.* (2002) and Hill & Thompson (2005) used CASI, HyMap and LiDAR data for landscape modelling applying a parcel-based approach in an English field-based landscape configuration. Although the data was pixel compatible after pre-processing, the data fusion took place at the feature level. The parcels were segmented using CASI. The parcel spectral properties were used for identification. LiDAR data were used to calculate additional parcel properties and assisted the segmented CASI data in identifying different woodland types. This approach worked well in a patchy cultural landscape but seems not applicable for classifying heterogeneous patches of natural vegetation.

Hudak *et al.* (2002) estimated canopy height at unsampled locations by LiDAR based on the statistical and geostatistical relations between the LiDAR data and a Landsat ETM+ image at sample locations. In this process, the canopy height is extracted from the LiDAR data and is subsequently correlated to the ETM+ image. This is considered a feature level data fusion.

Currently no results have been published combining and processing IS and LiDAR data at the pixel level. Fusing the data from these two sensor types could contribute to vegetation maps with classes separated on vegetation type and vertical structure as required for modern nature and river management. The idea of transforming the raw LiDAR data into one or several data layers, added as extra layer(s) to an IS image, seems a straightforward way to fuse datasets. To extract features, the fused data can be processed by standard classification algorithms, thus making the process readily available and cost effective.

The aim of this paper is to combine IS and LiDAR data by data fusion at the pixel level to improve the classification accuracy of an 8-class and 5-class set of natural vegetation types. The 8-class set represents the vegetation classes relevant for nature and river management, while the 5-class set serves as a minimum set to estimate hydraulic resistance for river management purposes. The classification results of the fused data are compared to classification results of IS only and LiDAR only of the same dataset.

## 2. Materials and Methods

A case study area was chosen along the Waal River; one of the main branches of the river Rhine in the Netherlands (Figure 1). The nature area consists of former fields and grasslands, which have been bought from farmers through time. Between 1990 and 1994 the nature area was formed and ever since the site has been left to develop itself under a regime of natural grazing. The surface area of the research area is 5.8 hectares and it contains mixed patches and ecotones, i.e. the transitions between plant communities, of grass, herbaceous vegetation, some bushes and part of a 40 year old softwood forest (Bekhuis *et al.* 1995, Sýkora 2002).

Insert Figure 1.

Table 1 lists the characteristics of the CASI data set. To cover the whole study area, two CASI flight lines were mosaiced using the mosaic function in Erdas Imagine (Erdas, 2005). The original geo-rectification of the CASI data proved insufficiently accurate (error of about 5 to 8 m or 3 to 4 pixels) and was re-georectified using a standard photogrammetrically generated river map of scale 1:1000 with planimetric error of 0.06 m (Anonymous 2003). To conserve the original DN values, nearest neighbour resampling was applied. The geo-rectification resulted in a root mean square (RMS) error of 2 m in x- and y-direction, i.e. about one pixel.

The LiDAR dataset of the study area was flown on 12$^{th}$ of October 2001 using an ALTM 2033 scanner. The first return pulse was recorded. This first return may be the result of a hit of the laser pulse somewhere on a vegetation layer (or even the top) or a hit on the ground if no vegetation is hit. The dataset was delivered as an ASCII file containing xyz coordinates. The mean density in the resulting dataset is about 1 point per square meter. The approximate elevation error is 0.07 m and the planimetric error less than 0.5 m. The elevation error was determined using standard test surfaces (total 270m$^2$) close to the research area (Brügelmann 2003). The planimetric error was determined using building perimeters from the same standard river map as used in the CASI geo-rectification (Anonymous 2003).

Insert table 1.

Field data on the floodplain vegetation were collected in August 2002 by botanists as part of a long term monitoring programme. The vegetation differences between the field data collection period (August 2002) and the date of flight (August and October 2001) can be considered negligible (Sýkora 2002). Within the monitoring programme, the plots were classified into 24 plant communities in accordance with the communities described by Schaminée *et al.* (1995) using TWINSPAN (Hill 1979). Additional bush and forest plots were added bringing the total to 405 plots in 25 classes which were used for classification and accuracy assessment.

The distinction of 25 vegetation classes is unnecessary for river management purposes and large-scale nature management. Furthermore, the number of plots is too low for a statistically sound classification into 25 classes. Therefore, the 25 original vegetation classes were regrouped into two related classification sets based on increasing vertical structure (Table 2). The vertical structure of vegetation is most important because it relates to the hydraulic resistance of the vegetation (van Velzen *et al.* 2003). The 5-class set (classes A to E) serves as a minimum set to estimate hydraulic resistance for river management purposes. In this set, herbaceous vegetation represents a large group of plant communities and is divided over classes B and C. Class B contains low herbaceous vegetation and class C contains higher herbaceous vegetation. The 8-class set provides more detail in the lower vegetation types and can be considered a minimum set for nature management purposes.

Insert table 2.

The classification procedure consisted of the following steps: (1) pre-processing of the LiDAR data and subsequently the fusion of the CASI and LiDAR data; (2) classification of the LiDAR data, the CASI data and of the fused image, and (3) evaluation of the results. These steps are explained in more detail below. Step 1 is illustrated in a flowchart (Figure 2).

Insert Figure 2

**Pre-processing of LiDAR data and fusion with CASI data**

A digital elevation model (DEM) was created and subtracted from the LiDAR data (vector points) to correct for variations in ground level. Per 2x2m pixel the lowest point in an area of a 10 metre search radius was chosen to represent the ground level and used to create the DEM. After subtraction of the DEM, the resulting LiDAR data was assumed to reflect variations in vegetation height only (step A in Figure 2; Figure 3a). The vegetation's vertical structure was described using the following statistics derived from the vegetation height points: minimum, maximum, mean, median, range and standard deviation (step B in Figure 2). These statistics (or 'textural bands') were computed for every 2x2m cell in the research area (matching the CASI raster cell size), using a 'moving window' operation (Figure 3a and 3b, Lillesand and Kiefer 2000, ESRI 2005). This yielded 6 LiDAR based rasters each containing one textural band, these bands were stacked (step C in Figure 2).

The number of LiDAR-points in the 'moving window' is defined by the size of the search radius (Figure 3b). If the radius is chosen too small, it will result in insufficient data points to calculate the required statistics. If it is chosen too large, it will smoothen the image detail. To test this, four stacked LiDAR raster sets were derived using search radii of 2 m, 3 m, 4 m and 6 m, respectively. The average number of LiDAR points per radius ranged from 13.8 (± 8.8 SD) for 2 m to 81.3 (± 51.9 SD) for 6 m. The variances in LiDAR point density are relatively high due to high concentration of LiDAR points in small borderlines of the flight paths where points per column range up to 160 for the 2 m search radius.

The data-fused image was created by stacking the layers in Erdas Imagine (Erdas 2005). Before stacking, the grid size of the CASI and pre-processed LiDAR data was reduced to 0.5 m to minimise the potential impact of a grid shift during the stacking procedure.

The fused images contained the 10 CASI bands and the 6 LiDAR texture bands and the cell size is 0.5 m. Four final fused-images were tested of which only the LiDAR bands differed: CASI fused with LiDAR bands derived from point statistics in a search area radius of 2 m, 3 m, 4 m and 6 m.

**Classification**

Maximum likelihood classification (MLC) was chosen to classify the data (Lillesand and Kiefer 2000, Thomas *et al.* 2003). MLC is a proven and robust method which gives a straightforward approach to classify and compare the different generated images and has been used previously to classify texture, e.g. by Liapis *et al.* (1997), Maas (1999) and Haack and Bechdol (2000).

All the bands of the fused image were normalised prior to classification by using a standard deviation stretch of 2 times the standard deviation (Mather 2004, Erdas 2005). Figure 4 shows an excerpt of the normalised fused image (LiDAR search radius 4 m) with the maximum vegetation height in red, green reflectance values in green and blue reflectance values in blue.

Insert figure 4.

The field data were split in two halves by spatially stratified random selection, resulting in separate training and testing sets for the MLC procedure. The training set was used to produce the signature files for MLC. Pixels within 3m of the centre point of the botanical field plots (3x3m) were considered representative for the plot. The test set was used to derive error matrices, to calculate overall accuracies (Kappa Average, overall percentage) and to produce maps. MLC was performed in Erdas Imagine (Erdas 2005).

**Evaluation**

The quality of the classification results was evaluated using conventional indicators such as error matrices, overall accuracy, Kappa and the Kappa-Z-test (Congalton 1991, Congalton 1999, Mather 2004). Furthermore, a new indicator was used which is referred to as the balance index (BI). The BI accounts for the fact that a misclassification between thematically distant classes (e.g. bare soil and forest) is considered worse than confusion of neighbouring classes (e.g. grass and herbaceous vegetation). The BI is calculated as the product of an error matrix (M) and a balance matrix (V) (Equation 1). If the error matrix is an $n$ x $n$ matrix, the balance matrix is an $n$ x $n$ matrix with maximum values (equalling $n$-1) on the top-left to bottom-right diagonal. The balance matrix is used to value the amount of misclassification and its values decrease towards the top-right and bottom-left corners (Equation 1). The product of the error and balance matrices is normalised by the maximum score possible, i.e. $n$-1 times the number of test plots (Equation 2). The result is a value between 0 and 1, where a value of 1 indicates a perfect classification and a value of 0 indicates the worst possible classification from the thematic distance point of view.

$$V = \begin{matrix} n-1 & .. & .. & .. & .. & .. & .. & 0 \\ .. & .. & .. & .. & .. & .. & .. & .. \\ .. & .. & n-1 & n-2 & n-3 & n-4 & .. & .. \\ .. & .. & n-2 & n-1 & n-2 & n-3 & .. & .. \\ .. & .. & n-3 & n-2 & n-1 & n-2 & .. & .. \\ .. & .. & n-4 & n-3 & n-2 & n-1 & .. & .. \\ .. & .. & .. & .. & .. & .. & .. & .. \\ 0 & .. & .. & .. & .. & .. & .. & n-1 \end{matrix} \qquad (1)$$

$$BI = \frac{\sum (M \times V)}{(n-1) \times \sum M} \qquad (2)$$

The BI is only applicable when, as in Table 2, the vegetation classes are ordered according to their vertical structure: from bare soil and pioneer vegetation (class A) to forest (class E), or any other principle of order. Only then the distance between a misclassified pixel and the diagonal is related to the amount of misclassification. This misclassification is valued by using the balance matrix. Two examples are given. Error matrices A and B both have an overall accuracy of 80 percent, i.e. 40 out of 50 test plots accurately classified, and only differ in the amount of misclassification. $V_{n=5}$ is the Balance matrix for a 5x5 error matrix, it values the classified pixels according to their distance from the diagonal. The Balance Indexes for A and B are computed as shown below; values for $BI_A$ and $BI_B$ are respectively 0.95 and 0.90.

$$A = \begin{matrix} 8 & 2 & 0 & 0 & 0 \\ 1 & 8 & 1 & 0 & 0 \\ 0 & 1 & 8 & 1 & 0 \\ 0 & 0 & 1 & 8 & 1 \\ 0 & 0 & 0 & 2 & 8 \end{matrix} \qquad B = \begin{matrix} 8 & 0 & 2 & 0 & 0 \\ 0 & 8 & 0 & 2 & 0 \\ 1 & 0 & 8 & 0 & 1 \\ 0 & 2 & 0 & 8 & 0 \\ 0 & 0 & 2 & 0 & 8 \end{matrix} \qquad V_{n=5} = \begin{matrix} 4 & 3 & 2 & 1 & 0 \\ 3 & 4 & 3 & 2 & 1 \\ 2 & 3 & 4 & 3 & 2 \\ 1 & 2 & 3 & 4 & 3 \\ 0 & 1 & 2 & 3 & 4 \end{matrix}$$

$$BI_A = \frac{\sum (A \times V)}{4 \times \sum A} = \frac{(5 \times 8 \times 4 + 10 \times 3)}{4 \times 50} = \frac{190}{200} = 0.95$$

$$BI_B = \frac{\sum (B \times V)}{4 \times \sum B} = \frac{(5 \times 8 \times 4 + 10 \times 2)}{4 \times 50} = \frac{180}{200} = 0.90$$

## 3. Results

Tables 3, 4 and 5 show the error matrices for the classification into 8 vegetation classes using only the CASI bands, only the LiDAR bands (of the 4 m search area radius image), and using both CASI and LiDAR bands, respectively. The columns show the distribution of the ground truth plots over the vegetation classes. The rows show the composition of the MLC results. Producers Accuracy and Users Accuracy are indicated as respectively PA and UA. The PA summarises the probability of a vegetation plot being correctly classified. The UA represents the probability of a classified pixel belonging to the class it represents (Congalton, 1991). Error matrix results for the images based on 2 m, 3 m and 6 m search area LiDAR statistics are not separately given but their results are summarised in Tables 6 and 7. Tables 6 and 7 show the Kappa index per class and the overall indexes Kappa Average, accuracy percentage and balance index for the 8-class and condensed 5-class set, respectively.

Insert Tables 3 to 7.

The overall CASI results were average (8-class set) to good (5-class set) with overall accuracies of 57.8% and 74% (Tables 6 & 7). CASI classification results were average to good for classes A, D and E (Tables 3 & 6). PA was low for classes B1 and B2; their plots were distributed over classes B1 to C2. UA was lowest for class B1.

Overall LiDAR results of the 8-class set and the 5-class set were poor (Tables 4 & 6). The confusion between the classes with smaller vegetation structure (A to C2) was large, clearly represented in the low class-specific Kappa values (Table 6) and the LiDAR (4 m) UA of class A (17%) and C1 (17%; Table 4). Structurally well-defined classes like bush (D) and forest (E) show good results.

For some classes all test plots are misclassified, i.e. zero on the diagonal in the corresponding error-matrices, this results in the negative class-specific Kappa values found in Table 5.

When comparing the results for the different LiDAR sets, the overall accuracy and Kappa index show a downward trend with an increasing search radius. The class-specific Kappa indexes show different trends per class: classes B1 and B2 have their optimum in the 3 m set, B3 and C2 have their optimum in the 2 m set and C2 and D in the 4 m set. The balance index is highest for the 3m set.

The overall results of the fused CASI and LiDAR data are average for the 8-class set (highest overall accuracy 63.5%) to good (81%) for the 5-class set. In all cases, the fused image had higher Kappa and overall accuracies than the CASI, but these differences were not significant at $p < 0.01$ (Kappa Z-test). For the 8-class (4m) and 5-class set, the differences were significant at $p<0.26$ and $p<0.19$ respectively. The fused image always performed significantly better than LiDAR ($p<0.01$). Generally, the results in the fused CASI and LiDAR error matrices were more balanced when compared to the error matrices of LiDAR and CASI alone, i.e., the confusion with distant classes decreased as shown in the balance index (Tables 6 & 7). The final maps for the 8-class set are shown in Figure 5. The heterogeneity of the area can be clearly recognised in these maps.
Figure 6 illustrates the performance in shadows. When using CASI only, the shadows are classified as Forest or Bush. In the fused image result, the shadows are classified as lower vegetation.

Insert Figure 5.
Insert Figure 6.

## 4. Discussion

In this study, LiDAR and CASI data were combined using a pixel-based method. The principle of pixel-based fusion worked well for this CASI and LiDAR dataset. Although the approach can be refined, the transformation of the LiDAR data into a layered grid containing LiDAR point statistics proved to be useful. The LiDAR data became an integral part of the image (Figure 4) and were easily used in existing classification algorithms and GIS applications, making it a readily available, labour efficient, reliable and cost effective method.
The LiDAR only approach used in this study performs well as a 3-class instrument: bare soil, grasses and herbaceous vegetation (A to C2) as one class, and bush (D) and forest (E) as another two classes. Confusion is high between classes with a relatively low vegetation structure. Asselman (2001) and Asselman *et al.* (2002) reached a similar conclusion for grassland vegetation.
The LiDAR results in Table 6 show that an increase of the search radius leads to a decrease of the overall accuracy. This can be explained by the smoothening effect that occurs at larger search radii. The accuracy of the classification of the individual vegetation classes, indicated by the class-specific Kappa index, does not always decrease with an increasing search radius. The vegetation classes have an optimum that seems related to the spatial variability within the class. The length of the search radius has little influence for bare soil & pioneer vegetation (A) which is relatively homogeneous over large areas. Vegetation that is variable on a small scale level is classified best using a 2 or 3 m radius (e.g. classes B1-C1: grassland and herbaceous vegetation), but vegetation that forms bigger homogeneous patches performs best using a 4 m radius (e.g. C2-D: herbaceous & low woody vegetation and bush). Forest patches have lowest kappa for the 2 m search radius and perform best at larger search radii.
The CASI data produced much better results than the LiDAR data. The classification accuracies obtained in this study (57.8 % for the 8-class set and 74 % for the 5-class set) are comparable to previous studies (60 to 80% overall accuracy for classification into 6 to 9 vegetation classes, Green *et al.* 1998, Thomas *et al.* 2003, Leckie *et al.* 2005). However, it should be noted that other studies deal with relatively homogeneous vegetation structures (i.e., patchy fields) when compared to the heterogeneous floodplain vegetation used in the study at hand. For the classes bush and

forest, the CASI data produced less accurate results than the LiDAR data. To estimate the hydraulic resistance for river management, the discrimination of bush and forest is of major importance. Geerling and Van den Berg (2002) also showed that spectral discrimination of bush and forest with CASI can be difficult, probably because both classes mainly consist of Willow (*Salix* spp).

From the LiDAR perspective, adding spectral data to the LiDAR data improved the results by more than 25% in the 8-class set to a 40% improvement in the 5-class set. Especially discrimination of low vegetation such as grasses and bare soil improved. The higher balance index indicates that confusion with distant classes diminished.

From the CASI perspective, adding LiDAR data to CASI data improved the overall classification accuracy up to 7 percent. Especially the classes with a well-defined structure, such as bush and forest, were classified more accurately when compared to CASI only. These are classes with a high hydraulic resistance and, as such, very important for the river manager. The results of our study are in line with Mundt *et al.* (2006) who found an improvement of 14% accuracy in the classification of sagebrush (*Artimisia tridentate Spp. wyomingensis*) after adding LiDAR to spectral data.

A common problem encountered in the classification of spectral data is misclassification due to shadows (Leckie *et al.* 2005). Figure 6 illustrates that this misclassification is reduced after fusion of the CASI and LiDAR data. It can be concluded that the classification of shady areas in the fused image is dominated by the added height information contained in the LiDAR texture bands, instead of the spectral information contained in the CASI bands.

The 2 m LiDAR set resulted in the highest overall accuracy and Kappa indexes of all LiDAR sets (Table 6). Remarkably, the results of its fusion with the CASI data were lowest. The 4 m LiDAR set produced the best results after fusion. These findings indicate that the classification of a fused image is not simply the sum of the separate CASI and LiDAR classifications. The MLC calculates the class probabilities for each pixel using the multivariate normal distribution fitted over the training set, with the values of the CASI and/or LiDAR bands as input values. The addition of extra bands to a pixel can influence the classification in different ways. If the extra bands have a low distinctive power, the calculated class probabilities will more or less remain unchanged. If the extra bands have a high distinctive power, the calculated class probabilities will increase for the pixel values falling within the range of high probability density, but will decrease for pixel values outside this range. However, a decrease or increase in class probability does not automatically imply that a pixel will be classified in a different class. This also depends on the change in probability for the other classes because a pixel is classified in the class with the highest probability. Addition of extra bands will only result in a different class if the new probability calculated for the original class is exceeded by that of another. This combination of changing (absolute) class probabilities and classification according to relative probabilities makes it particularly difficult to predict the classification results of the fused image based on the results of the separate CASI and LiDAR images. Nonetheless, some tendencies can be observed. The results in Table 6 indicate that the LiDAR bands have a large distinctive power for high vegetation classes, i.e. classes D and E. The CASI bands have a relatively large distinctive power for classes A, B3 and C1. Classes B1, B2 and C2 performed relatively poor in the CASI set and produced variable results in the 2, 3, 4 and 6 m LiDAR set. These varying LiDAR results seem to provide an explanation for the fact that the fused 2 m LiDAR image performed worse than the fused 4 m LiDAR image. In the 2 and 6 m LiDAR sets, classes B1, B2 and C2 performed worst; the kappa indexes of zero or lower indicate that the average class probability of the pixels for their true class

is lower than for the other classes. The 3 m LiDAR image performs well for classes B1 and B2, but this is counterbalanced by a bad performance for class C2. The 4 m LiDAR performs relatively well in all three classes, which may explain why the fused image with the 4 m LiDAR has the highest overall classification accuracy. Remarkably, classes B1 and B2 perform best in the 3 m LiDAR image before fusion, but after fusion they perform best in the fused image with the 4 m LiDAR. This illustrates that the performance of the fused image cannot easily be predicted based on the performance of the separate CASI and LiDAR images.

**Classifier**

In this study, a maximum likelihood classifier was used, but there are several other options available. A test with the same dataset using neural network and CART decision tree classifiers produced similar results (Psomas 2003). Using another part of the same CASI flight line, promising results were generated while developing new unsupervised classification algorithms, but these results were not tested against ground data (Tran *et al.* 2003). Another option is segmentation (Hill *et al.* 2002, Hill and Thompson, 2005). This approach is suitable for classification of large-scale patchy landscapes, but it seems less suitable for small-scale heterogeneous vegetation as found in the case study area. The 'soft borders' or transitions between plant communities encountered within semi-natural vegetation are difficult to segment. Therefore, a pixel-based approach seems more appropriate.

**Input data**

The LiDAR only results were relatively poor in the lower vegetation types. Firstly, a higher LiDAR point density could improve the classification because a better discrimination in classes with similar height is expected as the 3D structure is better recorded. In addition, when using higher density data, the search area (Figure 3) can be optimised for different vegetation types because the number of LiDAR points in smaller search areas will be sufficient for reliable statistics. However, the collection of high density LiDAR data may be constrained by the footprint size, which currently equals 25 to 40 cm for a small footprint (Reutebuch 2003).

Secondly, LiDAR signals are often reflected multiple times because of its footprint. The last return pulse is the reflection of that part of the beam which has travelled the longest distance, hence is more likely to be a ground level point. The LiDAR dataset used in this study contained only first return pulse values and was used for DEM and vegetation classification. The combined use of first and last return pulses can be expected to improve the quality of the DEM and the classification results. Especially for the detection of smaller objects, the accuracy of the DEM becomes more important. The generation of accurate DEMs out of LiDAR datasets is subject of extensive study (Cobby *et al.* 2001, Reutebuch *et al.* 2003).

Before classification a 2 times the standard deviation stretch normalisation was applied to the CASI and LiDAR fused images due to the difference in range of digital number between the CASI and LiDAR data. The visualisation of the images improved after this. Upon classifying a none normalised dataset with MLC, the results were identical. The MLC method is insensitive to differences in ranges as it calculates the class probabilities for each pixel using the multivariate normal distribution fitted over the training set. When using other classification algorithms, normalisation can influence the results. An example is classification with neural networks; the bands are normalised by pre-processing functions before the neural model is trained (Psomas 2003).

As mentioned in the Materials and Methods, the CASI data used consists of data from two flight lines. The use of multiple flight lines can have effects on the classification results due to differences of atmospheric condition, imaging condition and illumination geometry between these flight lines. Cross flight line radiometric normalisation can improve the results. In this research, one of the two CASI flight lines covers about 95% of the research area and contains 403 of the 405 plots used for training and testing. Effects on the results are considered minimal.

**Differentiation of input**

Classification of vegetation was realised in one step, but a natural landscape consists of elements of different scale. In the case study area, forest typically is of large scale and natural grasslands are of small scale because they contain heterogeneous patches of grasses and herbs. The area needed for representative sampling varies accordingly: the plot size needed for a representative area of forest typically is 10-30 metre, while the plot size of grassland typically is 2-5 metre. As shown, the ML classifier classifies the major differences between forest, bush, and small-scale vegetation when using the LiDAR data only, i.e. the LiDAR image results in 3 broad classes. More subtle differences might be too small for a single classification step. Based on the above, the landscape could be divided into large-scale and small-scale elements, and these elements could be treated separately in ML classification. This could improve the discrimination between smaller differences. This approach of separating the landscape in different scale levels and subsequently the use of ML classification is in fact a mix of a decision tree and ML classification.

**Geometric accuracy**

Geometric accuracy is of major importance when two independently acquired data sources are fused (Hill and Thompson 2005, Mundt *et al.* 2006). In this study the planimetric accuracy of the LiDAR data was higher than of the CASI data, which is a general problem when combining high resolution spectral and LiDAR data. For accurate results the use of combined sensors, acquiring multi sensor data at the same time, and so minimising co-registration errors, is highly favoured.

Another aspect favouring combined sensors is resampling of input data. While preparing and fusing the two different datasets, the CASI data was resampled during geo-rectification and stacking. Nearest neighbour resampling was chosen, so the original DN values of the CASI remained unaltered and because of its straightforwardness. Other resampling methods such as bilinear interpolation and cubic convolution, compute a DN value out of neighbouring pixels and so change the measured DN values but yield a visually smoother image (Mather 2004). As there are drawbacks to every resampling method, the number of times an image is resampled should be minimised to preserve image detail and reduce possible negative effects on the image classification results. Recording images the same time eliminates at least one of the resampling steps.

**Reliability of botanic field data**

The remote sensing community often regards botanic field data as hard facts. However, there are two sources of subjectivity enclosed in the botanic field data:

The botanic classification of plant species into 25 different plant classes was originally developed for plant science purposes and is subsequently used in nature conservation and management. It is inevitably based on arbitrary borders between classes. This botanic classification might not be the optimum for remote sensing purposes (Thomas *et al.*, 2003). The relation between botanic classification of plant species and classification of remotely sensed vegetation is topic of ongoing research.

The botanic field data used in the present study originates from field plots. The plots were classified (Hill 1979) on the basis of the plot's plant composition until they could be assigned to a botanic class described in Schaminée *et al.* (1995). Obviously, the assignment of classes to field plots involves some level of expert judgement by the botanist. Especially when a plot contains a mixture of different vegetation types, the assigned class will not always accurately reflect the heterogeneous nature of the vegetation within a plot.

**Data collection**

Collecting LiDAR data for vegetation purposes solely is expensive. However, lower density LiDAR is already systematically being used for the creation of DEMs. Combination of these purposes will make application of LiDAR for vegetation studies more feasible. For CASI images, a similar argument counts. If future digital scanners combine high resolution and Infra Red data, these images can be used as a substitute for aerial photographs (which are applied in plan processes of the river manager) and at the same time provide data for vegetation classification.

## 5. Conclusions

Fusion of CASI and LiDAR data can improve the classification of floodplain vegetation. Firstly, the overall accuracy is higher and the classification of shadows has improved. Secondly, the fused dataset classification shows diminished confusion with distant classes, i.e. the results become more balanced. This reduces errors in overall vegetation roughness when the maps are used as input in hydrological models. The best classification results of the fused data do not necessarily follow from the combination of separate sets with highest overall accuracy. They depend on the per-class added value of the probability distribution. It is expected that the classification results can be further improved by (1) using higher density LiDAR data, (2) the combined use of first and last return pulses, (3) the division of the landscape into large-scale and small-scale elements and subsequent classification and (4) optimising the botanic clustering of plant communities. The balance index proved to be a useful indicator for classification quality which takes into account the distance between classes.

**Acknowledgements**

Thanks to Division East and Survey Department of the Ministry of Transport, Public Works and Water Management for kind permission to use the CASI and LiDAR data. Many thanks to Prof. Dr. Karle Sýkora of Wageningen University for contributing his field data and advice. Thanks to Regine Brügelmann and Madelein Vreeken-Buijs, the project leaders of Ministry of Public Works and Transport, Survey Department, Delft. Also thanks to Achilleas Psomas for his discussions and valuable input. This project was funded by the Ministry of Public Works and Transport, Survey Department, Delft.

**References**

ACKERMANN, F., 1999, Airborne laser scanning - present status and future expectations. *ISPRS Journal of Photogrammetry and Remote Sensing*, **54**, 64-67.

ANONYMOUS, 2003, Product specification Digital Topographical Dataset – River (Dutch: Digitaal Topgrafisch Bestand – Nat) (Delft: Ministry of Transport, Public Works and Water Management. Directorate-General of Public Works and Water Management. Survey Department (AGI)).

ASSELMAN, N. E. M., 2001, Laser altimetry and hydraulic roughness of vegetation (Delft: WL | delft hydraulics).

ASSELMAN, N. E. M., MIDDELKOOP, H., RITZEN, M.R., and STRAATSMA, M. W., 2002, Assesment of the hydraulic roughness of river floodplains using laser altimetry, The structure, function and management implications of fluvial sedimentary systems, F. J. Dyer, M. C. Thoms and J. M. Olley (Eds.), *IHAS Publication* **276,** 381-388.

BAPTIST, M. J., PENNING, W. E., DUEL, H., SMITS, A.J.M., GEERLING, G.W., VAN DER LEE, G.E.M., VAN ALPHEN, J.S.L., 2004, assessment of the effects of Cyclic Floodplain Rejuvenation on flood levels and biodiversity along the Rhine river. *River Research & Applications*, **20**, 285-297.

BEKHUIS, J., BOSMAN, W. , and WOESTHUIS, H., 1995, *Millingerwaard, Development report of years 1993-1994, In Dutch* (Laag Keppel: Ark Foundation).

BRÜGELMANN, R., 2003, *Quality test of the LiDAR dataset. Internal document.* Personal Communication (Delft: Ministry of Transport, Public Works and Water Management. Directorate-General of Public Works and Water Management. Survey Department (AGI)).

CHARLTON, M.E., LARGE, A.R.G., and FULLER, I.C., 2003, Application of Airborne lidar in river environments: the River Coquet, Northumberland, UK. *Earth Surface Processes and Landforms*, **28,** 299-306.

COBBY, D. M., MASON, D. C., and DAVENPORT, I.J., 2001, Image processing of airborne scanning laser altimetry data for improved river flood modelling. *ISPRS Journal of Photogrammetry and Remote Sensing*, **56,** 121-138.

CONGALTON, R. G., 1991, A review of assessing the accuracy of classifications of remotely sensed data. *Remote Sensing of Environment*, **37,** 35-46.

CONGALTON, R.G., Green, K., 1999, *Assessing the Accuracy of Remotely Sensed Data: Principles and Practices*. (Boca Raton, Florida, US: Lewis Publishers.).

DOWLING, R. and ACCAD, A., 2003, Vegetation classification of the riparian zone along the Brisbane river, Queensland, Australia, using light detection and ranging (lidar) data and forward looking video. *Canadian Journal of remote sensing*, **29,** 556-563.

ERDAS, 2005, *Erdas Imagine 8.7. Tour Guide*. (Atlanta, Georgia: Erdas Inc.).

ESRI, 2005, *ArcGIS 9.1 and ArcInfo workstation*. (Redlands: Environmental Systems Research Institute).

GEERLING, G. W. and VAN DEN BERG, G. J., 2002, *Monitoring and Dynamic River Management. In Dutch* (Nijmegen: Department of Environmental studies, section nature management of river corridors, University of Nijmegen and Delft: Ministry of Transport, Public Works and Water Management, Directorate-General of Public Works and Water Management, Survey Department (AGI)).

GEERLING, G.W., RAGAS, A.M.J., LEUVEN, R.S.E.W., VAN DEN BERG, J.H., BREEDVELD, M., LIEFHEBBER, D. and SMITS, A.J.M., 2006, Succession and rejuvenation in floodplains along the River Allier (France). *Hydrobiologia* 565: 71-86.

GREEN, E. P., MUMBY, P. J., EDWARDS, A. J., CLARK, C. D. and ELLIS, A. C., 1998, The assessment of mangrove areas using high resolution multispectral airborne imagery. *Journal of Coastal Research*, **14**, 433-443.

HAACK, B. and BECHDOL, M., 2000, Integrating multisensor data and RADAR texture measures for land cover mapping. *Computers & Geosciences*, **26,** 411-421.

HILL, M. O., 1979, *TWINSPAN - A FORTRAN program for arranging multivariate data in an ordered two-way table by classification of individuals and attributes*, (Ithaca, N.Y.: Cornell University).

HILL, R.A., SMITH, G.S., FULLER, R.M., VEITCH, N., 2002, Landscape modelling using airborne multispectral and laserscanning data. *International journal of remote sensing*, **23**, 2327-2334.

HILL, R.A. and THOMPSON, A.G., 2005, Mapping woodland species composition and structure using airborne spectral and LiDAR data. *International Journal of Remote Sensing*, **26**, 3763-3779.

HUDAK, A. T., LEFSKY, M. A., COHEN, W. B. and BERTERRETCHE, M., 2002, Integration of lidar and Landsat ETM+ data for estimating and mapping forest canopy height. *Remote sensing of Environment*, **82**, 397-416.

KURNATOWSKA, A. M., 1998, Large-scale vegetation mapping in mountain environments using remote sensing and plant physiology methods. In *Operational Remote Sensing for Sustainable Development*, Nieuwenhuis, G. J. A., Vaughan, R. A. and M. Molenaar (Eds.) (Lisse: Balkema), pp. 61-65.

LECKIE, D.G., CLONEY, E., JAY, C. and PARADINE, D., 2005, Automated mapping of stream features with high resolution multispectral imagery: an example of the capabilities. *Photogrammetric Engineering & Remote Sensing*, **71,** 145-155.

LENDERS, H. J. R., 2003, Environmental rehabilitation of the river landscape in the Netherlands. A blend of five dimensions. PhD thesis, University of Nijmegen.

LEUVEN, R. S. E. W., POURDEVIGNE, I. and TEEUW, R. M., 2002, Remote sensing and Geographic Information Systems as emerging tools for riverine habitat and landscape evaluation: from concepts to models. In *Application of Geographic Information Systems and Remote Sensing in River Studies*, Leuven, R. S. E. W., Pourdevigne, I. and Teeuw, R. M. (Eds.) (Leiden: Backhuys Publishers).

LIAPIS, S., ALVERTOS, N., TZIRITAS, G., 1997, Maximum likelihood texture classification and Bayesian texture segmentation using discrete wavelet frames. In *International Conference on Digital Signal Processing*, 2-4 July 1997, Santorini, Greece (http://ieeexplore.ieee.org), pp. 2:1107-1110.

LILLESAND, T. M. and KIEFER, R. W., 2000, *Remote sensing and image interpretation* (New York: John Wiley & Sons, Inc.).

MAAS, G.H., 1999, The potential of height texture measures for the segmentation of airborne laser scanner data. In *Fourth International Airborne Remote Sensing conference and Exhibition / 21st Canadian symposium on Remote Sensing*, 21-24 June 1999, Ottawa, Ontario, Canada.

MATHER, P. M., 2004, *Computer processing of remotely sensed images, an introduction*. (Chichester, West Sussex, England: John Wiley & Sons Ltd.).

MUNDT, J.T., STREUTKER, D.R. and GLENN, N.F., 2006, Mapping sagebrush distribution using fusion of hyperspectral and lidar classifications. *Photogrammetric Engineering & Remote Sensing*, **72**, 47-54.

POHL, C., and VAN GENDEREN, J.L., 1998, Multisensor image fusion in remote sensing: concepts, methods and applications. International journal of remote sensing, **19**, 823-854.

PRACH, K. and PYSEK, P., 2001, Using spontaneous succession for restoration of human-disturbed habitats: Experience from Central Europe. Ecological Engineering **17,** 55-62.

PROTZ, R., VAN DEN BYGAART, A.J., WOOD, M. D. and HULFHOF, B.G.A., 1999, Evaluation of high resolution airborne imagery and global positioning systems for monitoring changes in agro ecosystems. RES/MON-012/97, COESA.

PSOMAS, A., 2003, *Vegetation mapping of floodplain areas by means of Artificial Neural Networks*. MSc thesis report GIRS-2003-18. (Wageningen: Centre for Geo-Information, Wageningen University and Research).

REUTEBUCH, S.E., MCGAUGHEY, R.J., ANDERSEN, H.E. and CARSON, W.W., 2003, Accuracy of high resolution lidar terrain model under a conifer forest canopy. *Canadian Journal of Remote Sensing* **29**, 527-535.

SCHAMINÉE, J.H.J., STORTELDER, A.H.F.,WESTHOFF, V., 1995, *The vegetation of the Netherlands. Introduction to plantsociology: basics, methods and applications (In dutch)*. (Upsala and Leiden: Opulus Press).

SHANG, J., JOLLINEAU, M. Y., HOWARTH, P. J. and J. WANG, 1998, A comparison of spatial- and spectral-mode CASI imagery for coastal wetland mapping in the Lake St. Clair delta: preliminary results. In *The 20th Canadian Symposium on Remote Sensing*, 10-13 May, Calgary, Canada, pp. 215-218

SMITS, A. J. M., NIENHUIS, P. H. and LEUVEN, R. S. E. W., 2000, *New Approaches to River Management* (Leiden: Backhuys Publishers).

STRAATSMA, M.W. and MIDDELKOOP, H., 2006, Airborne laser scanning as a tool for lowland floodplain vegetation monitoring. *Hydrobiologia*, **565**, 87-103.

SUAREZ, J.C., ONTIVEROS, C., SMITH, S., SNAPE,S., 2005, Use of airborne LiDAR and aerial photography in the estimation of individual tree heights in forestry. *Computers and Geosciences*, **31**, 253-262.

SÝKORA, K., 2002, *On vegetation surveys and succession in the floodplain Millingerwaard, Waal river, the Netherlands. Research data. Personal Communication* (Wageningen: Wageningen University, Nature Conservation and Plant Ecology Group, Chair: Ecological Construction and Management of Infrastructure).

THOMAS, V., TREITZ, P., JELINSKI, D., MILLER, J., LAFLEUR, P. and MCCAUGHEY, J. H., 2003, Image classification of a northern peatland complex using spectral and plant community data. *Remote Sensing of Environment*, **84**, 83-99.

TRAN, T. N., WEHRENS, R. and BUYDENS, L. M. C., 2003, SpaRef: a clustering algorithm for multispectral images. *Analytica Chimica Acta*, **490**, 303-312.

TURNER, W., SPECTOR, S., GARDINER, N., FLADELAND, M., STERLING, E. and STEININGER, M., 2003, Remote sensing for biodiversity science and conservation. *Trends in Ecology and Evolution*, **18**, 306-314.

VAN DER VELDE, G., LEUVEN, R.S.E.W., RAGAS, A.M.J., SMITS, A.J.M., 2006, Living rivers: trends and challenges in science en management. *Hydrobiologia* 565: 359-367

VAN VELZEN, E., JESSE, P., CORNELISSEN, P., COOPS, H., 2003, *Hydraulic resistance of floodplain vegetation (in Dutch), parts 1 and 2* (Arnhem: Ministry of Transport, Public Works and Water Management, Directorate-General of Public Works and Water Management, Institute for Inland Water Management and Waste Water Treatment (RIZA)).

VON HANSEN, W. and STIES, M., 2000, On the capabilities of digital high resolution multispectral remote sensing techniques to serve nature conservation requirements. *International archives of Photogrammetry and Remote Sensing* XXXIII(Part B7).

WEHR, A. and LOHR, U., 1999, Airborne laser scanning - an introduction and overview. *ISPRS Journal of Photogrammetry and Remote Sensing*, **54**, 68-82.

WOLFERT, H. P., 2001, *Geomorphological Change and River Rehabilitation*, PhD thesis, Alterra Green World Research.

ZIMBLE, D.A., EVANS, D.L., CARLSON, G.C., PARKER, R.C., GRADO, S.C., GERARD, P.D., 2003, Characterizing vertical forest structure using small-footprint airborne LiDAR. *Remote Sensing of the Environment*, **87**, 17, 1-182.

## Figures

Figure 1. The Location of the study area in the Netherlands along the Waal River, a Rhine branch.


Figure 2. Flowchart showing the general procedure for pre-processing of the raw LiDAR data and the pixel based fusion of CASI and LiDAR data.

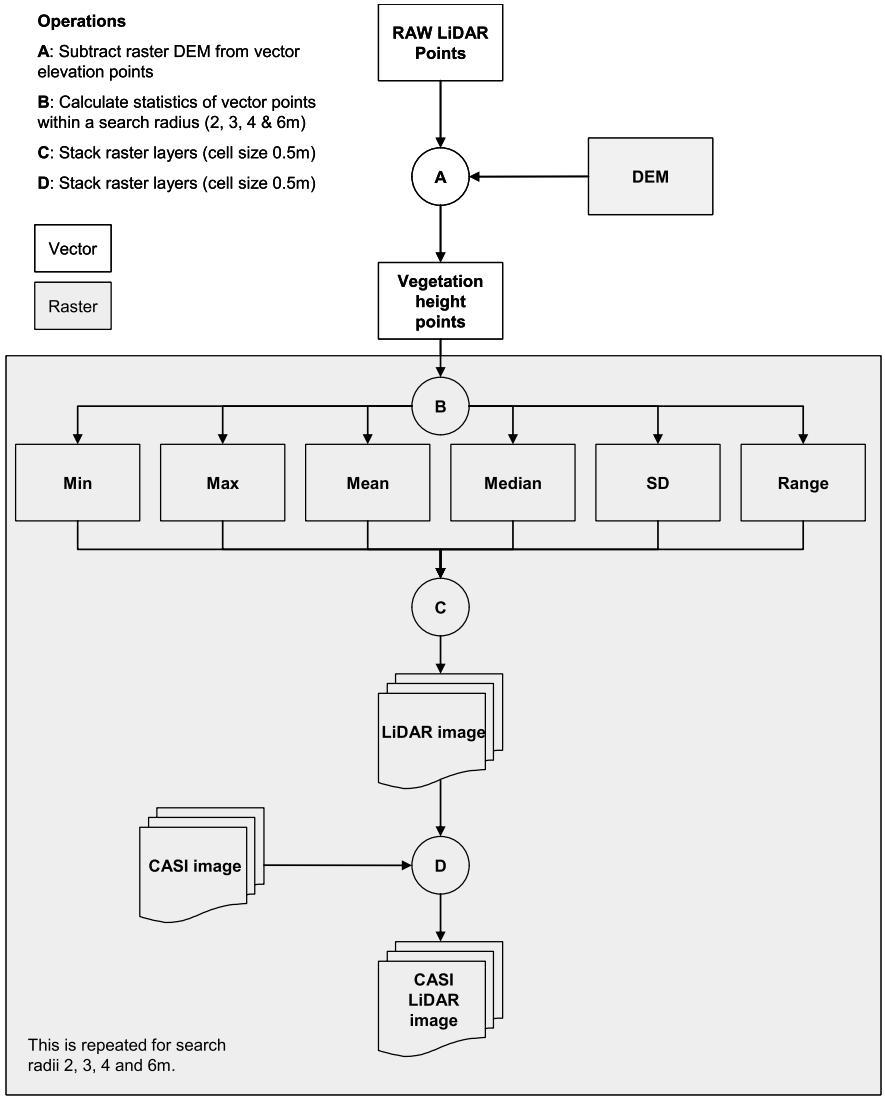

Figure 3a. Example of LiDAR point clouds of training plots of classes Bush (D) on left and Forest (E) on the right. Points fall into a circular search area which are depicted as black circles overlaid on the DEM.

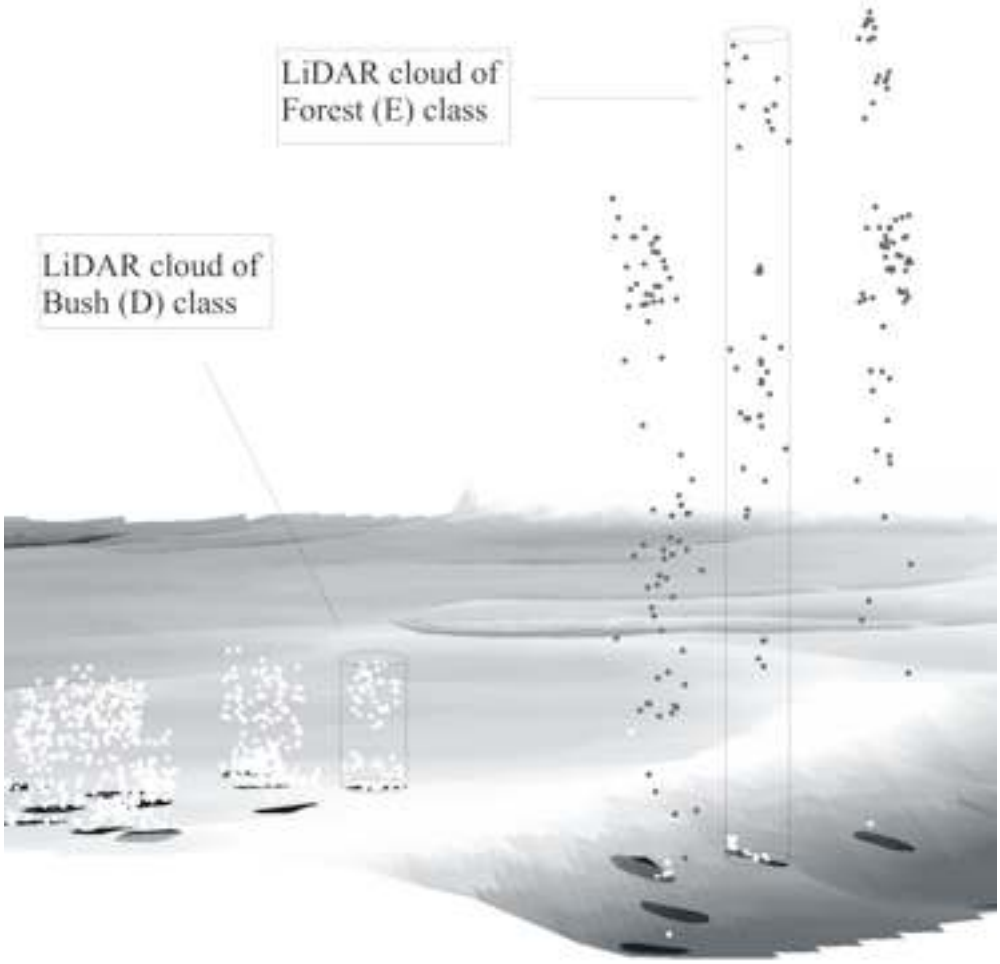


Figure 3b. Preparation of LiDAR texture statistics min, max, mean, median, standard deviation and range. The scattered dots represent the LiDAR point cloud from above. The grid is according to the CASI grid and the circles represent the search area.

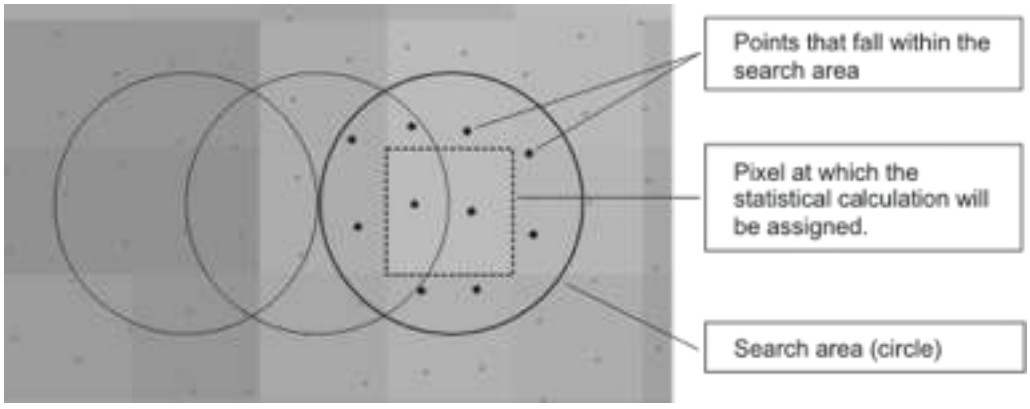

Figure 4. Example of the fused CASI and LiDAR image. Of the 16 band image (10 CASI and 6 LiDAR texture bands) 3 bands are shown, indicating the potential of data-fusion. RGB values correspond to maximum vegetation height, and reflectance of band (549-559 nm) in green and the band (437-447 nm) in blue. The bushes (dark red) and trees (bright red) stand out in this band combination. The light blue-ish line is a sandy path.

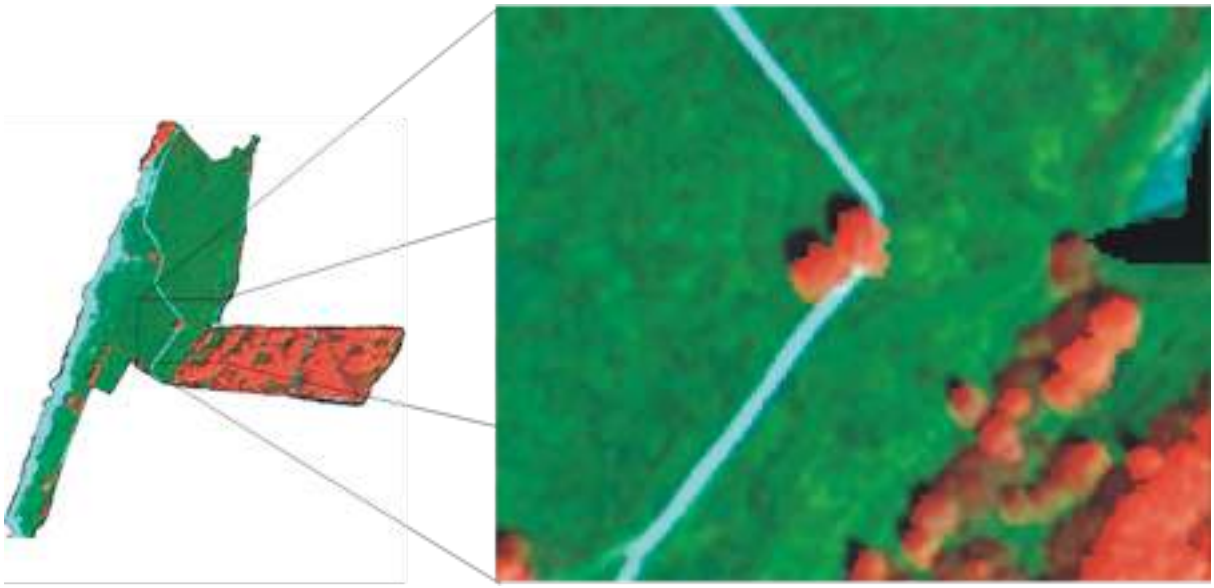

Figure 5. Maps of classification results LiDAR (4m), CASI, and Fused CASI LiDAR (4m).

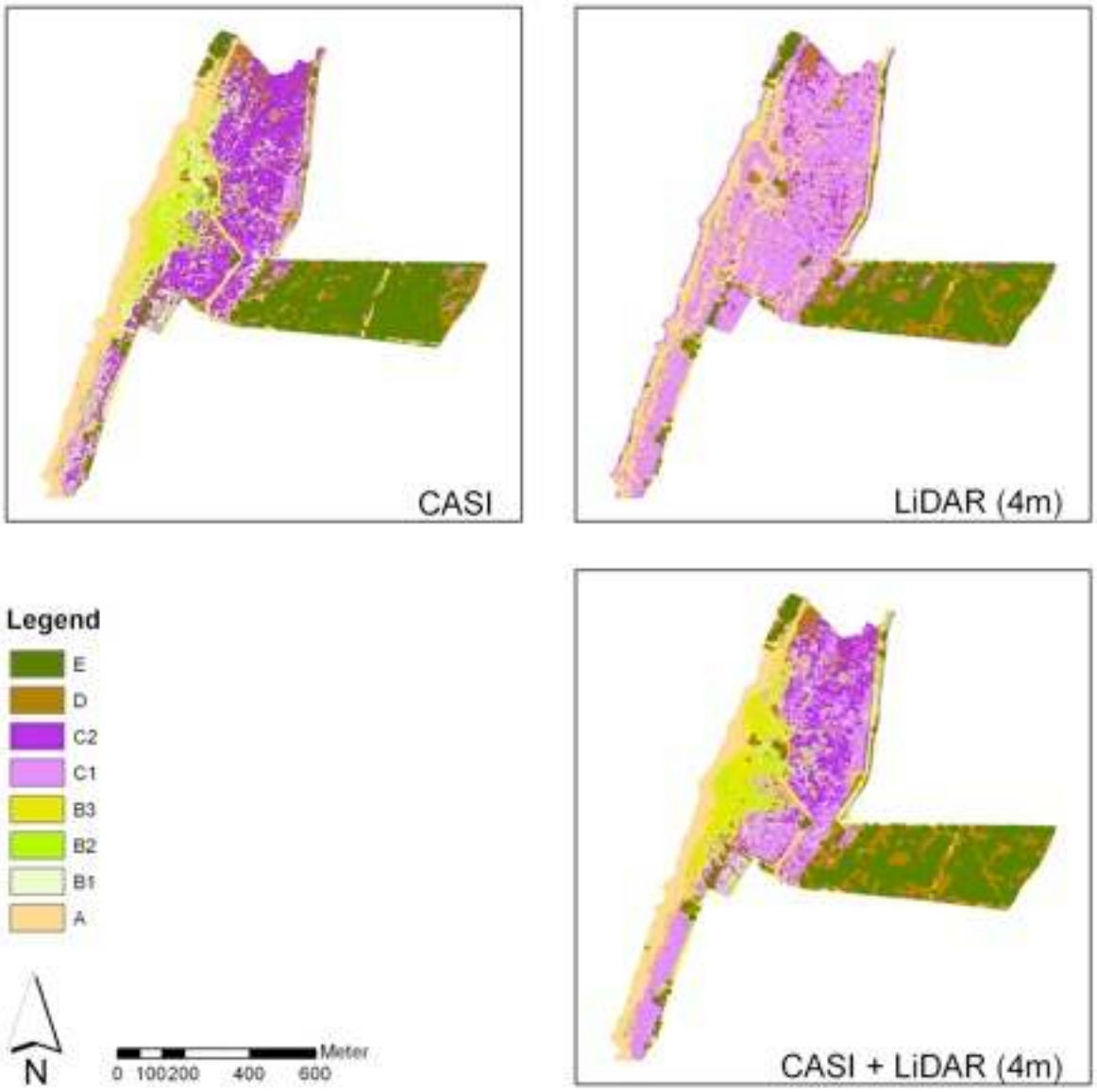

Figure 6. Two examples of classification of shadows. On the left, a true colour image (CASI bands 615-625 nm (red), 549-559 nm (green) and 437-447 nm (blue)) on which the shadows are outlined in red. The middle image shows shadows mainly classified as trees in the CASI classification . On the right, shadows classified using the fused CASI LiDAR data appear partly as tree (covered in shadow) and partly as surrounding lower vegetation.

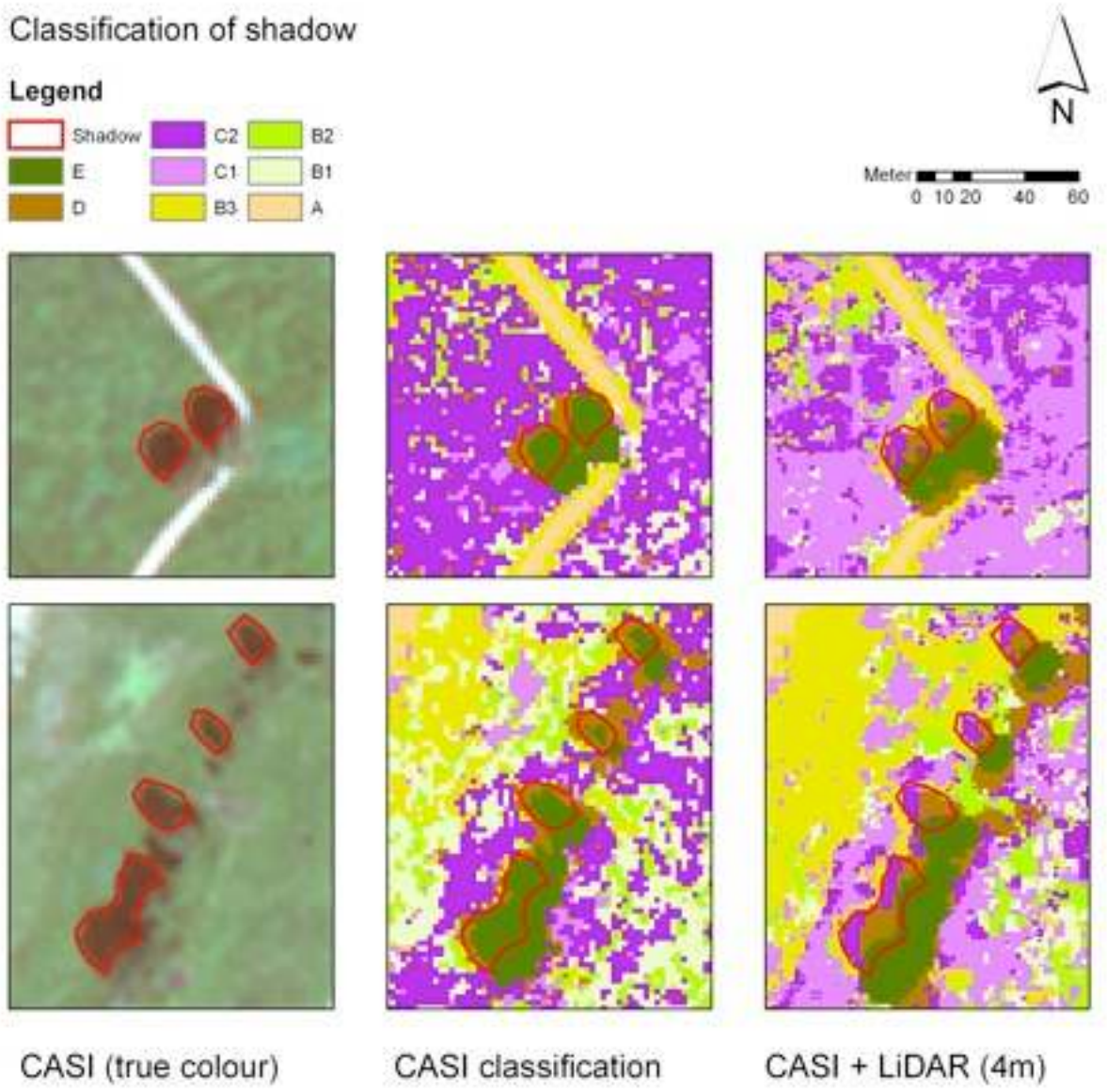

Table 1: Specification of the Compact Airborne Spectral Imager (CASI) data used.

| | |
|---|---|
| Date of Flight | 15 august 2001 |
| Flight elevation | 1500m |
| Swath width | 1536m |
| Pixel size*) | 2m |
| Number of spectral bands | 10 |
| Spectral range | 437-890 nm |

*) The original pixel size was 3m but resampled to 2m by the imaging company; the original 3m data was unavailable for this study

Table 2. Classes used for classification. The plant communities are used from Sýkora (2002) and described in Schaminée *et al.* (1995). Some plant communities are preceded by RG which is Romp Gemeenschap (Dutch) meaning "fragmented community". When plant communities are preceded by RG, this means that the communities found did not always contain all community species, i.e., were not fully saturated, and sometimes consisted of overlapping communities.

| 5 class set | 8 class set | Plant communities |
|---|---|---|
| A<br>Bare and pioneer communities | A | Chenopodietum rubri<br>Fragmented Medicagini-Avenetum pubescentis / Fragmented Bromo inermis-Eryngietum campestris<br>Lolio-Potentillion anserinae / Fragmented Bromo inermis-Eryngietum campestris<br>RG of *Cirsium arvense* en *Polygonum amphibium* [Artemisietia vulgaris] |
| B<br>Grasses and herbaceous vegetation | B1 | Fragmented Medicagini-Avenetum pubescentis / Bromo inermis-Eryngietum campestris with *Cynodon dactylon*<br>Fragmented Ranunculo-Alopecuretum geniculati with *Trifolium repens*<br>RG of *Cynodon dactylon* + *Euphorbia esula* [Sedo-Cerastion] / Fragmented Bromo inermis-Eryngietum campestris |
| | B2 | Fragmented Arrhenatheretum elatioris<br>Fragmented Medicagini-Avenetum pubescentis / Bromo inermis-Eryngietum campestris with *Oenothera erytrosepala* and *Sedum acre*<br>Fragmented Ranunculo-Alopecuretum geniculati |
| | B3 | Bromo inermis-Eryngietum campestris<br>Bromo inermis-Eryngietum campestris / fragmented Medicagini-Avenetum pubescentis<br>Fragmented Medicagini-Avenetum pubescentis / Bromo inermis-Eryngietum campestris with *Euphorbia cyparissias* and *Medicago falcata*<br>Rorippo-Oenanthetum aquaticae |
| C<br>Herbaceous and low woody vegetation | C1 | Fragmentair Ranunculo-Alopecuretum geniculati<br>Ranunculo-Alopecuretum geniculati<br>RG of *Brassica nigra* [Phragmitetea] / Fragmented Ranunculo-Alopecuretum geniculati<br>RG of *Calamagrostis epigejos* and *Epilobium hirsutum* [Galio-Urticetea]<br>RG of *Mentha aquatica* and *Lycopus europaeus* [Narsturtio-Glycerietalia] |
| | C2 | Fragmented Ranunculo-Alopecuretum geniculati / RG of Rubus caesius [Phragmitetea]<br>RG of *Rubus caesius* [Galio-Urticetea]<br>RG of *Urtica dioica* [Galio-Urticetea] |
| D<br>Bush | D | RG *Sambucus nigra* [Galio-Urticetea]<br>RG of *Ulmus minor* [Galio-Urticetea] |
| E<br>Forest | E | RG of Urtica dioica [Salicion albae] |

Table 3. The error matrix of the classification using only the CASI bands of the fused image, based on a separate test set. Producers Accuracy (PA) and Users Accuracy (UA) are shown.

| | Reference data | | | | | | | | |
|---|---|---|---|---|---|---|---|---|---|
| Classified data | A | B1 | B2 | B3 | C1 | C2 | D | E | UA |
| A | **11** | 2 | 0 | 2 | 2 | 0 | 0 | 0 | 65% |
| B1 | 0 | **8** | 5 | 7 | 4 | 3 | 0 | 0 | 30% |
| B2 | 0 | 0 | **7** | 8 | 0 | 2 | 0 | 0 | 41% |
| B3 | 3 | 6 | 5 | **31** | 0 | 3 | 0 | 1 | 63% |
| C1 | 0 | 2 | 3 | 2 | **12** | 1 | 1 | 0 | 57% |
| C2 | 0 | 5 | 7 | 1 | 3 | **13** | 3 | 0 | 41% |
| D | 0 | 0 | 1 | 2 | 0 | 2 | **12** | 0 | 71% |
| E | 0 | 0 | 0 | 0 | 0 | 0 | 3 | **28** | 90% |
| PA | 79% | 35% | 25% | 58% | 57% | 54% | 63% | 97% | |

Table 4. The error matrix of the classification of only the LiDAR bands (in the fused image with search area 4m radius for LiDAR points), based on a separate test set. Producers Accuracy (PA) and Users Accuracy (UA) are shown.

| | Reference data | | | | | | | | |
|---|---|---|---|---|---|---|---|---|---|
| Classified data | A | B1 | B2 | B3 | C1 | C2 | D | E | UA |
| A | **6** | 6 | 4 | 15 | 3 | 1 | 0 | 0 | 17% |
| B1 | 0 | **1** | 2 | 0 | 0 | 0 | 0 | 0 | 33% |
| B2 | 4 | 2 | **5** | 1 | 0 | 3 | 0 | 0 | 33% |
| B3 | 1 | 1 | 5 | **4** | 0 | 2 | 0 | 0 | 31% |
| C1 | 3 | 13 | 12 | 33 | **16** | 16 | 0 | 0 | 17% |
| C2 | 0 | 0 | 0 | 0 | 2 | **2** | 3 | 0 | 29% |
| D | 0 | 0 | 0 | 0 | 0 | 0 | **16** | 1 | 94% |
| E | 0 | 0 | 0 | 0 | 0 | 0 | 0 | **28** | 100% |
| PA | 43% | 4% | 18% | 8% | 76% | 8% | 84% | 97% | |

Table 5. The error matrix of classification of both CASI and LiDAR bands (in the fused image with search area 4m radius for LiDAR points), based on a separate test set. The Producers Accuracy (PA) and Users Accuracy (UA) are shown.

| | Reference data | | | | | | | | |
|---|---|---|---|---|---|---|---|---|---|
| Classified data | A | B1 | B2 | B3 | C1 | C2 | D | E | UA |
| A | **11** | 2 | 0 | 2 | 2 | 0 | 0 | 0 | 65% |
| B1 | 0 | **6** | 1 | 0 | 1 | 0 | 0 | 0 | 75% |
| B2 | 0 | 1 | **15** | 7 | 0 | 4 | 0 | 0 | 56% |
| B3 | 3 | 10 | 5 | **40** | 3 | 2 | 0 | 0 | 63% |
| C1 | 0 | 3 | 5 | 4 | **13** | 13 | 0 | 0 | 34% |
| C2 | 0 | 1 | 2 | 0 | 2 | **4** | 3 | 0 | 33% |
| D | 0 | 0 | 0 | 0 | 0 | 1 | **16** | 0 | 94% |
| E | 0 | 0 | 0 | 0 | 0 | 0 | 0 | **29** | 100% |
| PA | 79% | 26% | 54% | 75% | 62% | 17% | 84% | 100% | |

Table 6. The per-class accuracies (Kappa index) and overall accuracy indexes (Kappa Average, Percentage and Balance) for all 8-class classifications. The distance value between brackets (2, 3, 4 and 6 m) refers to the search area radii used to compute the LiDAR statistics from the LiDAR points.

| | CASI | LiDAR (2m) | Fused (2m) | LiDAR (3m) | Fused (3m) | LiDAR (4m) | Fused (4m) | LiDAR (6m) | Fused (6m) |
|---|---|---|---|---|---|---|---|---|---|
| Class | | | | | Accuracy (Kappa) | | | | |
| A | 0.62 | 0.13 | 0.62 | 0.11 | 0.62 | 0.11 | 0.62 | 0.11 | 0.62 |
| B1 | 0.21 | 0.00 | -0.12 | 0.44 | 0.44 | 0.25 | 0.72 | -0.12 | 0.25 |
| B2 | 0.32 | 0.00 | 0.62 | 0.26 | 0.40 | 0.23 | 0.49 | 0.23 | 0.40 |
| B3 | 0.51 | 0.27 | 0.41 | 0.25 | 0.49 | 0.08 | 0.51 | -0.34 | 0.58 |
| C1 | 0.52 | 0.22 | 0.23 | 0.10 | 0.27 | 0.08 | 0.27 | 0.04 | 0.24 |
| C2 | 0.33 | 0.00 | 0.44 | -0.13 | 0.36 | 0.19 | 0.25 | 0.06 | 0.25 |
| D | 0.68 | 0.84 | 0.84 | 0.93 | 0.88 | 0.94 | 0.94 | 0.68 | 0.79 |
| E | 0.89 | 0.96 | 1.00 | 1.00 | 1.00 | 1.00 | 1.00 | 1.00 | 1.00 |
| Overall indexes | | | | | | | | | |
| Kappa Average | 0.51 | 0.36 | 0.52 | 0.33 | 0.55 | 0.29 | 0.57 | 0.23 | 0.53 |
| Accuracy % | 57.8 | 44.6 | 59.7 | 42.2 | 61.6 | 37.0 | 63.5 | 31.3 | 59.7 |
| Balance | 0.871 | 0.835 | 0.905 | 0.852 | 0.907 | 0.836 | 0.910 | 0.821 | 0.886 |

Table 7. The per-class accuracy (Kappa index) and overall accuracy (Kappa Average, Percentage and Balance) for the CASI, LiDAR (4m) and Fused CASI LiDAR (4m) 5-class classification. The distance value between brackets ( 4 m) refers to the search area radius used to compute the LiDAR statistics from the LiDAR points.

| | CASI | LiDAR (4m) | Fused (4m) |
|---|---|---|---|
| Class | | Accuracy (Kappa) | |
| A | 0.62 | 0.03 | 0.62 |
| B | 0.69 | 0.04 | 0.64 |
| C | 0.44 | 0.39 | 0.57 |
| D | 0.52 | 0.87 | 0.88 |
| E | 0.89 | 1.00 | 1.00 |
| | | Overall Indexes | |
| Kappa Average | 0.63 | 0.28 | 0.71 |
| Accuracy % | 74.4 | 41.2 | 80.6 |
| Balance | 0.929 | 0.835 | 0.948 |